*Computational Materials Science* 163 (2019) 176-185.

# Evolution of Solidification Defects in Deformation of Nano-Polycrystalline Aluminum

Avik Mahata[1] and Mohsen Asle Zaeem[1,2*]

[1] Department of Materials Science and Engineering, Missouri University of Science and Technology, Rolla, MO 65409, USA
[2] Department of Mechanical Engineering, Colorado School of Mines, Golden, CO 40801, USA

**Abstract**

Formation of solidification defects and their evolution in uniaxial tensile deformation of solidified polycrystalline aluminum (Al) were investigated by molecular dynamics (MD) simulations. First, solidification process was simulated both isothermally and with different quench rates. At the initial stages of nucleation, coherent twin boundaries and/or fivefold twins formed depending on the quench rate or the undercooling temperature. The solidified polycrystalline Al consisted of randomly distributed grains, twin boundaries, and vacancies. Evolution of nanostructures and defects in uniaxial tensile deformation of solidified Al under different temperatures and strain rates were studied. Void formation at grain boundaries and detwinning of preexisting solidification twins and deformation twins were observed during the uniaxial deformation. It was also found that the temperature of deformation has a stronger effect than the applied strain rate on the strength of solidified samples. For solidified cases with grain sizes lower than 10 nm, the yield strength and Young's modulus increased with increasing grain size, indicating an inverse Hall-Petch relationship. Similar to experimental data, MD simulations showed a higher yield strength for single crystal Al and a large plastic deformation for polycrystalline Al.

**Keywords**: Solidification; polycrystalline aluminum; defects; deformation mechanics; molecular dynamics.

*Corresponding author; email: zaeem@mines.edu (M. Asle Zaeem)

## 1. Introduction

Solidification plays a significant role in various manufacturing processes such as casting and additive manufacturing. The nano- and micro-structures that form during solidification determine the mechanical response and deformation behavior of solidified materials, which can be distinctly different from those of the single crystal counterparts. Study the process-mediated defects at the nanoscale and their effect on deformation and mechanical response of materials is very important for their reliable use in practical applications.

Crystal defects such as dislocations (one dimensional line defects) and twins (two dimensional planar defects) form in metallic materials during the solidification process. These defects play critical roles in facilitating plastic deformation and ultimately control various mechanical behaviors of most polycrystalline metals and alloys [1-3]. Formation of twin phases in metallic alloys by means of deformation has been reported quite frequently in the literature [4-8]. Formation of twins in solidified [9-11] and annealed [12-14] metals are also reported. The final grain structure after solidification is modified by multiple twins and they can affect the distribution of crystallographic orientations of grains in the ingot [15]. It is essential to know the evolution of twin structures as the solidification progresses. However, the initial stages of formation of twins during solidification have never been investigated in depth. Tracing the origin of the twin formation in a manufacturing process is extremely difficult because the real-time monitoring of nucleation and solidification process in metals and alloys at atomic scale is almost impossible experimentally [16-19].

Controlling factors such as strain rate (SR) and temperature during plastic deformation have critical effects on the deformation mechanisms (stacking faults, twinning, voids, dislocations, and grain boundaries). These factors also affect the mechanical properties of metallic systems. Usually dislocations govern the plastic deformation [20-22], but as grain size decreases the dislocation activity is suppressed by the grain boundaries (GBs) and twinning. When a critical average grain size is achieved, which was reported previously to be ~10 nm for Al [4, 23]), GB related phenomena and twinning become the primary deformation mechanisms.

In the particular case of aluminum (Al), first efforts to study solidification twins were done more than half a century ago [24, 25]. The study by Fredriksson and Hillert on Al showed how all the twin tips grow in the same (112) growth direction, and this gives the tip a favorable shape. By

producing sharp edges, feathery crystal growth is observed during continuous casting. This proposed twining process during solidification of Al has never been explained in depth. The study by Fredriksson and Hillert found a particularly interesting case to correlate twinning and feathery growth of Al, and they reported twin boundary motions in both (112) and (110) directions. Few other experimental studies reported both solidification and deformation twins in single crystal of Al [4, 12, 26]. Also, a previous study reported fivefold twining of Al during nanoindentation based on a quasicontinuum method [27]. Most studies related to twinning in Al are based on deformation induced twins, but studying twinning during solidification is also important in order to understand the origin and evolution of twins. However, five-fold twins are studied using MD simulations for some other metals such as Cu [28, 29] and Fe [30].

Materials with a high stacking fault energy (SFE) have difficulty undergoing twinning by deformation. Al for example with a high SFE of 104-142 mJ $m^{-2}$ has difficulty twinning [4, 31-34]. This is due to the much higher shear stress needed for nucleation of the twinning partial dislocations than the trailing partial dislocations , and also because of the large amount of slip systems in the fcc structure, which make the slip a dominant deformation mechanism [26, 35]. However, it has been shown that twinning in nanocrystalline Al is quite possible [32, 35, 36]. Plastically deformed Al with a thickness between 200 nm and 400 nm and an average grain size between 10 nm and 35nm [4] shows deformation twins, dislocations and stacking faults. The interplay between twinning, stacking faults and dislocations was also revealed extensively in nanocrystalline Al by MD simulations of tensile testing with a load of 2.5 GPa and at 300 K [35]. Nanocrystalline twinning can be explained by a dislocation based model. Glides of Shockley partial dislocations, with a Burges vector = $a_o$<112>/6 ($a_o$ is the lattice constant), on consecutive planes create multilayered intrinsic stacking faults which produces a twin [37]. Even though twinning in bulk Al is less common, twinning in nanocrystalline Al is frequently reported in the literature. Twinning is generally a permanent deformation, but under high SRs detwinning has been observed in Al [32, 38]. Detwinning is usually a two-step process. First, the twin boundaries come closer together causing the twin to get thinner, and then the twin boundaries will get shorter and eventually disappear [38].

In the literature, there are several studies done on deformation of polycrystalline metals by MD simulations. But in these studies, the polycrystalline metals were created artificially by

building the initial polycrystalline structure using Voronoi tessellation methods [39-42] or introducing multiple nanotwins [3, 8]. The artificially created GBs can have partial twins in their initial configuration. But majority of twins and dislocations appear when the deformation process starts. The initial type, amount and distribution of defects in previous MD simulations may not be comparable to those observed in experiments. In reality, the solidified metals have different type of defects and solidification twins. The other disadvantages of artificially created grains are that the initial twins and dislocations do not have any interactions with other defects other than the GBs.

In this work, we study twins that formed during solidification of Al melt and the deformation twins caused by deformation of nanocrystalline Al. The twinning defects are captured during crystal nucleation at the early stages of solidification and twinning growth directions are identified as the solidification proceeds. Due to formation of defects and GBs during the solidification, spontaneous formation of polycrystalline Al is achieved. The solidified polycrystalline Al is deformed by a uniaxial tensile load. The effect of solidification quenching rate, tensile testing temperature, and SR are investigated. Also, the evolution of defects (twinning, detwinning, and voids) are studied under different tensile loading conditions.

## 2. Computational Methodology

### 2.1 Interatomic potential

Second nearest neighbor modified embedded atom method (2NN-MEAM) potential is one of the most advanced and efficient semi-empirical interatomic potentials for predicting both low temperature properties (e.g., elastic properties, stable-unstable stacking fault energy, vacancy formation energy, and surface energy) and high temperature properties (e.g., thermal expansion coefficient, solid-liquid interface free energy, and melting point) of metals very accurately [34, 43-45]. The 2NN-MEAM was initially developed by Lee and Baskes [43], and recently we evaluated its performance in calculating high temperature and solid-liquid coexistence properties of Al [34, 46], showing good agreement with the experimental data. We used the OVITO to investigate nucleation, solidification and deformation processes [47]. The local crystalline environment of the crystalline atoms were studied by using common neighbor analysis (CNA) in OVITO [48]. The

CNA algorithm identifies the closet neighbor and calculate number of neighbor atoms, then group them as fcc, bcc, hcp or other crystal structures [48].

**2.2 Simulation details**

MD simulations of solidification and uniaxial deformation of solidified pure Al were completed using simulation boxes consisting of ~1 M atoms (25×25×25 $nm^3$ or 64×64×64 unit cells). We utilized periodic boundary conditions for solidification simulations and free boundary conditions for deformation simulations in all three directions. The time step of simulations was 0.003 ps. Nose-Hoover thermostat governed the temperature and the Parrinello-Rahman barostat to maintain the pressure [49]. We utilized the LAMMPS code [50] (Large-scale Atomic/Molecular Massively Parallel Simulator) for our MD simulations. The melt and a polycrystalline solidified structure are shown in Fig. 1. The melt (Fig. 1(a)) is equilibrated for 100 ps to create a homogenous liquid. As shown in Fig. 1(b), the solidified Al is having GBs and twin boundaries (TBs), which can be easily determined by visual investigation.

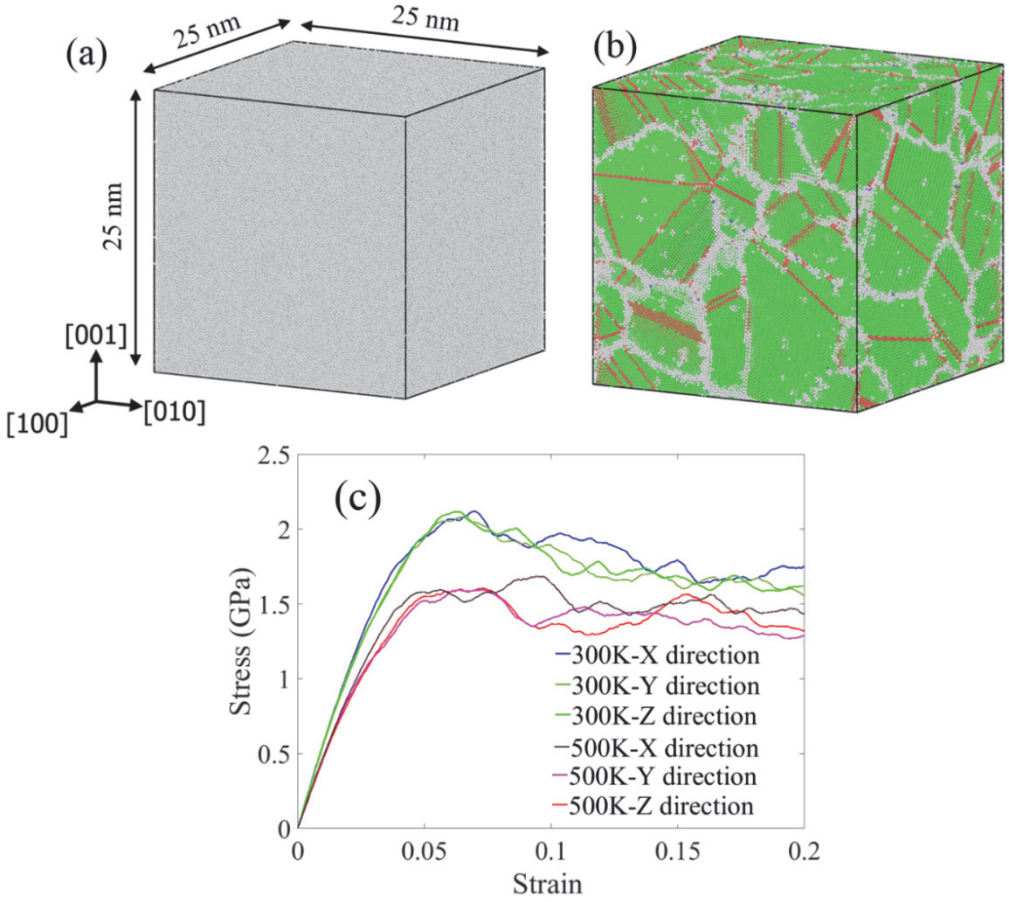


**Fig. 1.** Simulation box at (a) initial melt with temperature of 1,325 K, and (b) after the solidification with the quench rate of $2.5x10^{11}$ $Ks^{-1}$ to 300 K. Green atoms are fcc, and red atoms are hcp. Amorphous solid and liquid atoms are presented by grey color. (c) Stress-strain curves for tensile deformation in x, y and z direction at the strain-rate of $10^9$ $s^{-1}$; temperatures show the tensile testing temperature.

Solidified polycrystalline samples were prepared by both isothermal condition and quenching. The isothermal samples were prepared by keeping the Al melt at a constant undercooling temperature such as 300, 400 and 500 K for 3ns (3,000 ps). Average grain size increases with increasing the undercooling temperature. The results on the effect of undercooling temperature on the average grain size was provided in our previous work [46], showing that the average grain size increases with increasing the undercooling temperature. In a later part of our article, the grain-size dependent mechanical properties of Al are studied. In the same way, Al melt is quenched from a high temperature such as, 1,325 K to 300 K at constant cooling rates of $10^{11}$, $2.5\times10^{11}$ and $5\times10^{11}$ $Ks^{-1}$. Six polycrystalline samples are created, three for isothermal and three for quenching cases. All the polycrystalline Al models are deformed at three different deformation

temperatures (300, 400 and 500 K) and three SRs ($10^8$, $10^9$ and $10^{10}$ $s^{-1}$), as shown in Table 2. For the purpose of comparison, we also deform a single crystal Al at the same SRs and temperatures (9 cases). To calculate the statistical error from all the simulations, each uniaxial tensile simulation is replicated in (100), (010) and (001) directions. So, overall 195 simulations (6 solidification cases, and 63 deformation cases each at 3 directions) were performed to analyze the deformation behavior and mechanical properties of solidified polycrystalline Al.

Table 2. The quench rate and isothermal temperature of solidification cases, as well as the SR and temperature of deformation cases (54 deformation cases); a single crystal Al is also deformed at the same SRs and temperatures (9 cases). Each uniaxial tensile deformation simulation is replicated in (100), (010) and (001) directions.

| | |
|---|---|
| Quench rate of solidification | $10^{11}$ $Ks^{-1}$, $2.5\times10^{11}$ $Ks^{-1}$, and $5\times10^{11}$ $Ks^{-1}$ |
| Isothermal solidification at | 300 K, 400 K, and 500 K |
| SR ($s^{-1}$) | $10^8$, $10^9$, and $10^{10}$ |
| Deformation temperature | 300 K, 400 K, and 500 K |

The polycrystalline samples are prepared by spontaneous solidification. The location, size, and orientation of grains or twins are not controlled in this method. Due to the arbitrary locations of the GBs and TBs, each of the polycrystalline samples are deformed separately in three orthogonal directions to get the statistical scatter. Fig. 1(c) shows a sample that is created by isothermal solidification at 400 K, and then deformed at 300 K and 500 K with a SR of $10^9$ $s^{-1}$. For each tensile testing temperature, Fig. 1(c) shows slight differences in the elastic region, but more visible differences in the plastic region based on different directions. The difference in stress-strain curves indicates that the evolution of the pre-existing GBs and TBs are different and dependent on the applied load direction. Therefore, the statistical error from direction-dependence is considered in analyzing the mechanical properties of polycrystalline Al.

## 3. Results and Discussion

### 3.1. Formation of coherent and five-fold twins during rapid solidification

The magnified crystalline nucleus in Fig. 2(a-b) displays atoms with different crystal structures, calculated by CNA [48]. In Fig. 2 (a-b), the distance between two nearest-neighbor atoms in Al matrix is ~ 2.86 Å, and this is consistent with the lattice constant of 4.05 Å for Al. There is a small amount of thermal fluctuation of energy during the solidification of Al melt. The

fcc to hcp energy difference is only 0.03 eV whereas the fcc to bcc energy difference is 0.12 eV [34]. During solidification while thermal fluctuations happen, hcp stacking faults form in the Al system, and no bcc phase forms. Depending on the cooling rate, different types of twins form within the critical nuclei. In the quenching process when the crystallization occurs by homogenous nucleation, two types of twinning are observed. Fivefold twins form for the relatively higher quench rate of $2.5x10^{11}$ $Ks^{-1}$ (Fig. 2a), and coherent twin boundaries (CTBs) form for the quench rare of $10^{11}$ $Ks^{-1}$ (Fig. 2b). The isothermally solidified Al also shows fivefold twins for all the examined solidification temperatures. It takes about 60 ps from the formation of initial stacking faults to formation of fivefold twins. Unlike the multifold twins by deformation, the solidification twins are not assisted by sequential emission of Shockley partial dislocations. CTBs and multifold twins both form spontaneously in the fcc crystal nuclei during solidification. The twins grow further in the same direction of growth of the fcc crystalline solid.

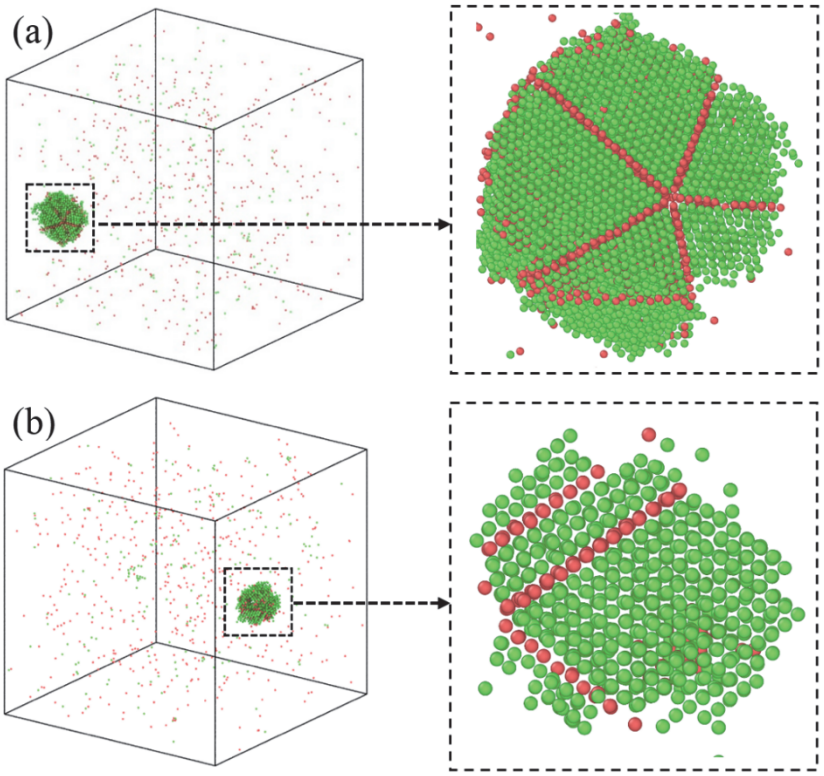


**Fig. 2.** Formation of (a) five-fold twins and (b) CTBs during solidification at the nuclei; the cooling rate is $2.5\times10^{11}$ $Ks^{-1}$ and $10^{11}$ $Ks^{-1}$, respectively. Green atoms indicate fcc, and red atoms are hcp. Amorphous solid liquid atoms are removed to only show the nuclei.

The instability in the solidification process caused by thermal fluctuations at solid-liquid interfaces is the only reason that creates the twins. In general, Al has a relatively high SFE which makes it difficult for twins to form in pure Al. But, this high theoretical SFE happens at 0 K. It is a well-known that SFE gradually decreases as the temperature increases [51, 52]. Recent studies by Bhogra et al. [53] showed that the SFE of Al reduces drastically by increasing the temperature. At higher temperatures, the SFE of Al is almost equivalent to that of Nickel (Ni) [54], and formation of fivefold twins was observed during electrodeposition of Ni thin films [55]. During solidification, crystal nucleation occurs at very high temperatures where SFE is significantly lower that its value at 0 K, thus formation of twins is probable.

In general the multifold twinning happens in different scenarios such as layer-by-layer growth during nucleation, successive growth twinning, or deformation twinning [55]. Twining during growth is observed in semiconductor growth process, but it is extremely difficult to experimentally observe the same for metals due to the much higher temperatures during solidification. The formation steps and direction of five-fold twins and the CTBs are presented in Fig 4(a-f). To study the formation of five-fold structure in the nucleus, we present only a sliced portion of the simulation box between 15-100 ps in Fig. 3. In the initial stages of nucleation, a solid cluster consisting of nearly 50 fcc and hcp atoms was formed at ~15 ps inside the undercooled Al met, which can be regarded as the seed for both the nucleus and the twin. Then the initial TB1 seed (hcp atoms) elongates and forms a complete TB1 while the nucleus becomes critical simultaneously. Between 30 and 45 ps, as the nucleus grows in size and TB2 began to form. Subsequently at ~45 ps, a lamellar twined structure with two hcp planes apart by 73 ° formed at the bottom right of the particle. The initial stage of formation of TB3 is noticeable by the extension of upper hcp plane to connect at the junction of TB1 and TB2, forming a three-fold twin. The TB4 and TB5 subsequently appears after ~60 ps, whereas TB1, TB2 and TB3 were still growing. At the three-point twin junction, the hcp atoms start forming two other TBs, namely TB4 and TB5. As the solidification proceeds, these twins are arranged into a closed five-membered circle at the twinning axis. Finally, the entire five-fold twins were formed at ~75 ps, when the TB4 and TB5 are fully stretched out.

The five-fold twins should be producing 360 ° while distributed in a circle, but the average twin angle remains in a range of 70 to 73 ° . The twins also has a thickness, which leave a gap

while closing 360 ° (Fig. 3(f)), and that later result in elastic strain during deformation. The result shows consistency with the literature values of other fcc metals [55-57]. Fivefold twin structure formations by successive twinning growth on alternate cozonal twin planes also has been previously observed in the solid phase crystallization of metal [52]. During the nucleation and growth of the noncrystallographic packing of atoms to a crystalline fcc Al, small size ordered subunits of hcp atoms form as a twin to compensate the angular misfit between different fcc growth planes.

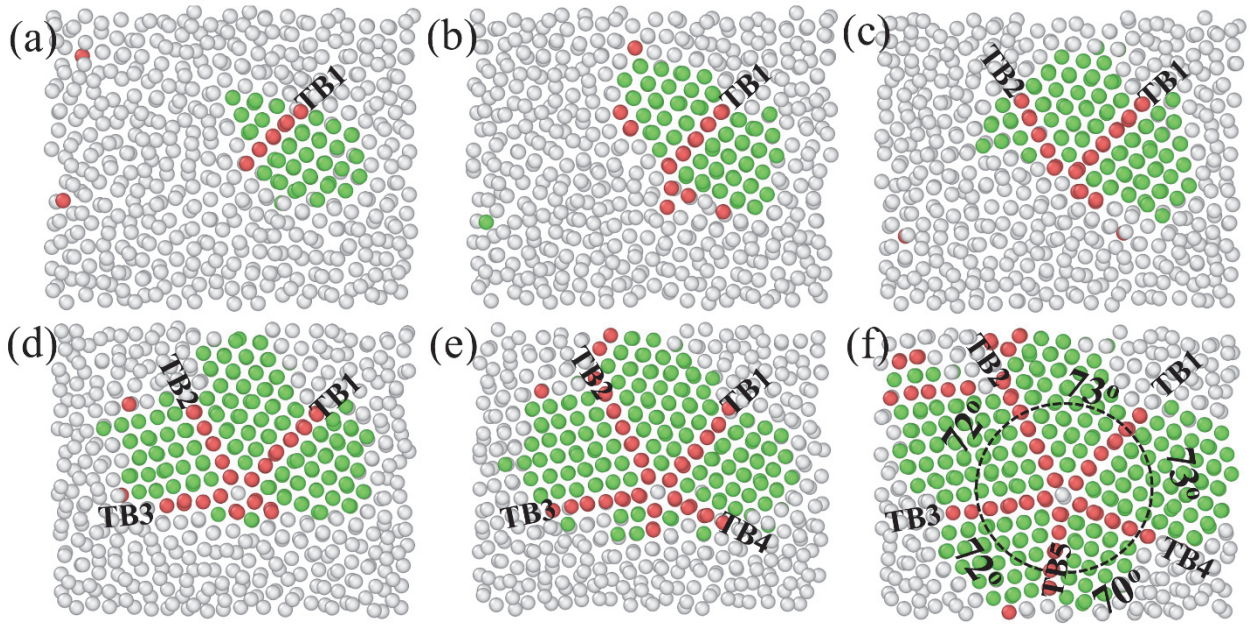


**Fig. 3.** The sequence of formation of (a-f) five-fold twins at the nuclei at 500 K isothermal temperature. The steps of twin formation is shown for (a) 15 ps, (b) 30 ps, (c) 45 ps, (d) 60 ps, (e) 75 ps and (f) 100 ps. The angle between the twins are measured which remains between 70 ° and 73 ° .

Along with the fivefold twins, several CTBs are also identified during both isothermal and quenching solidification (see Fig. 4 for example). Some initial CTBs occur within the fcc nuclei during solidification, Fig. 4(b). In the annealing stage, more twins form on the GBs, see Fig. 4(a) and Fig. 4(b) for example. Some TBs connect with each other at the GBs, see Fig. 4(c) and Fig. 4(d) for example. As the grain size increases with annealing, the smaller grains combine with the larger ones and some GBs vanish, and during this process some hcp TBs form within the fcc Al grains.

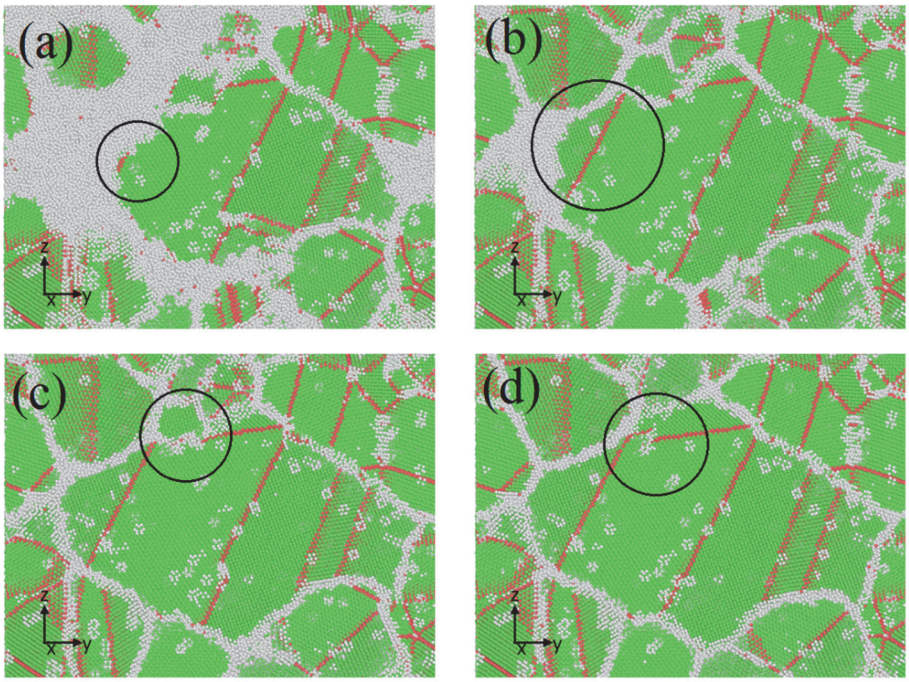


**Fig. 4.** The formation steps of coherent TBs at (a) 15 ps, (b) 50 ps, (c) 100 ps, (d) 250 ps at 400 K. The circles show the hcp TB formation and merger at a GB.

### 3.2. Twinning and detwinning during tensile loading

Several phenomena simultaneously happen during the tensile loading of polycrystalline Al. New deformation twins form and some of the preexisting solidification twins detwin. Then some of the deformation twins also detwin while the simulation box is stretched in a uniaxial direction. Along with the formation of usual CTBs, we also observed formation of several fivefold twins during the deformation. Snapshots of formation of a fivefold twin during deformation at 300 K and SR of $10^8$ $s^{-1}$ are revealed in Fig. 5; the initial nanostructures for this deformation simulation was for the solidification case with the quench rate of $2.5\times10^{11}$ $Ks^{-1}$. The angles between the TBs of the fivefold twin remain between 70 and 73°, which is similar to those of the fivefold twins in solidification cases. No fivefold twins were detected in planes perpendicular to the loading direction. Formation of Fivefold twins has been observed for several nanocrystalline materials during experimental deformation [58-60]. The arrow in Fig. 5(a) shows one of the preexisting solidification TB (TB1). This pretexting twin can be referred to as a microtwin, as it grows in length when the uniaxial tension applied. Below the TB1 several other twins are present but during the deformation some of them detwin by the GB movement; however, in this case one

of them forms the TB2 (shown in Fig. 5(b)). The emission of partial dislocations from GBs in different grains results in formation of other twins of the fivefold twin. By simply applying uniaxial tension in a perfect single crystal Al, multifold twins cannot be created, however by introducing pretwins in grain regions, multifold/fivefold deformation twins can form in grains of a nanocrystalline system which undergoes a uniaxial tension [61].

In Fig. 5 formation of several coherent and incoherent TBs can be seem as well. A pair of CTBs are shown in Fig. 5 with a dotted circle. The thickness (distance between two twin planes) of the TB reduces from ~2.23 nm at 0.15 strain to 1.35 nm at 0.25 strain. As shown in the dotted circle some gray atoms at the front end of the TB. These atoms can be referred to as partial dislocations [62, 63]. As shown in Fig. 5(c) and Fig. 5(d), a partial dislocation glides in the opposite direction of TB growth. Consequently, detwinning happens with a combination of both reduction in twin thickness and the layer-by-layer TB removal by the opposite glide of partial dislocations having a Burgers vector identical to that of the twinning partial dislocations.

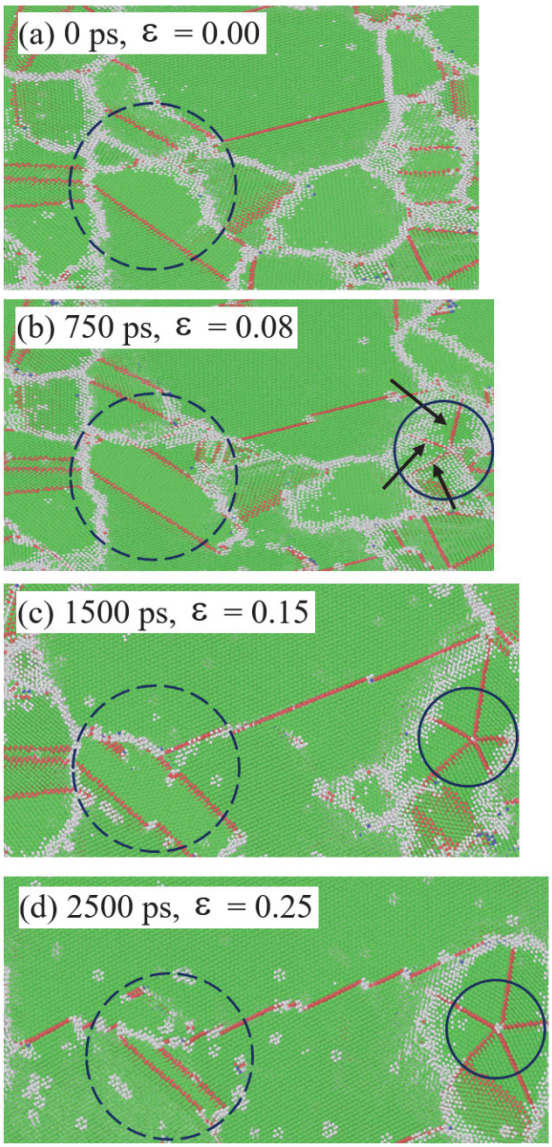


**Fig. 5.** Fivefold twin formation during tensile deformation (in x direction) of polycrystalline Al created from a quench rate of $2.5\times10^{11}$ $Ks^{-1}$ at SR of $10^{8}$ $s^{-1}$. The normal black circle shows the fivefold twin formation and the dotted circle shows the formation of CTB.

The solidification TBs detwin by GB movements and dissolution into to the fcc matrix, Fig. 6(a)-(d). Once TBs are present from the solidification process, the subsequent tensile deformation favors detwinning of the TBs over activating dislocation slip. Since the TBs are already present from the solidification defects, it is not required to generate new partial dislocations, and the trailing partial dislocations can dismantle the stacking fault on the TBs. In this particular case, which was solidified at 400 K and then deformed at 300K with SR of $10^{9}$ $Ks^{-}$

[1] (Fig. 6), the initial GB transformed to one CTB, then as the simulation box stretched up to total strain of strain ~0.45 (Fig. 6(d)), the TB dissolved back into the primary fcc Al matrix.

The deformation temperature influences the detwinning process. When the TBs dissolve into the fcc Al matrix, the detwinning process mostly happens due to the stretching of the TBs in the direction of applied uniaxial tension, and SR controls this process. But when the detwinning happens due to GB movement, the detwinning process is mostly influenced by the deformation temperature; as the temperature of deformation increases from 300 K to 500 K, the detwinning happens more frequently. Multiple twins at the GB are absorbed by both the GB and the fcc Al matrix. This detwinning phenomena is observed for all the different samples prepared by isothermal annealing or quenching. The detwinning process during deformation identified by MD simulations is similar to the results obtained from previous experimental works on various fcc metals such as Al , Cu , Ni [64], etc. So MD simulations of polycrystalline metals can replicate the detwinning observed in experiments such as thinning of the twins and shortening, and GB movement during deformation [38].

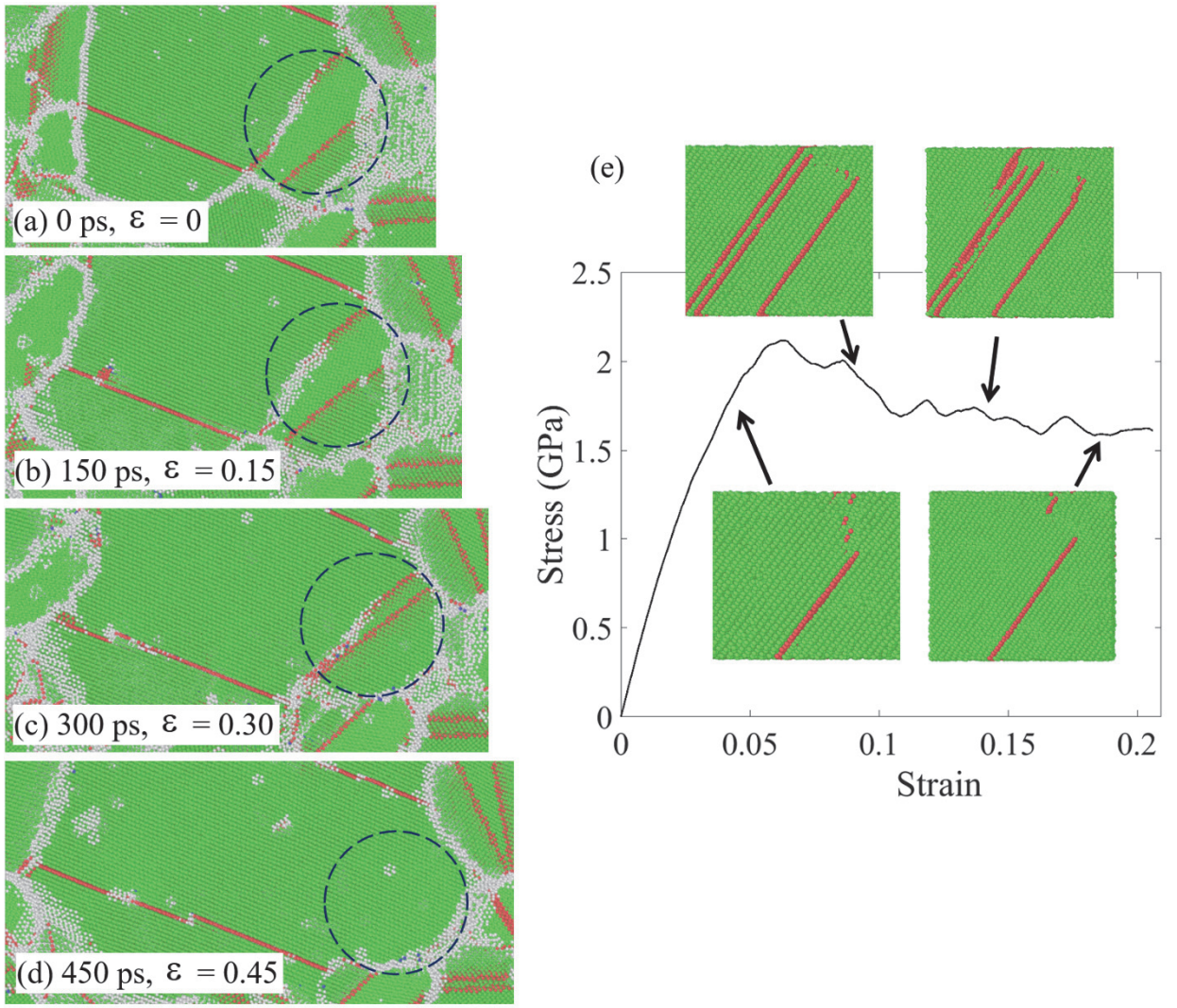


**Fig. 6.** A solidification twin detwin as tensile deformation in x direction proceeds. (a) The initial condition (t=0) is the nanostructure of an isothermally solidified sample at 400 K, and (b-d) the SR of $10^9$ $Ks^{-1}$ is applied at 300 K. (e) A typical Stress-strain plot of polycrystalline Al produced by 400 K isothermal annealing, deformed at SR of $10^9$ $s^{-1}$ and 300 K. The inset images shows twinning-detwinning during plastic deformation. The microstructures are removed for clarity.

Typical detwinning of deformation twins is observed while the sample is plastically deformed, which is similar to the observations in experimental work [38]. The stages of detwinning of deformation twins is similar to those of the solidification TBs. It should be noted that during the deformation only smaller sized TBs detwin. The small sized twins at high SRs do not entangle with other defects (such as dislocations and GBs) in the Al matrix. The length of TBs do not increase significantly during deformation due to the high SFE of Al [65] at low temperatures.

Some of the fivefold twins also detwin as the tensile deformation continues. The driving force behind the detwinning comes from the excess energy variation of the system during the tensile deformation. But for the detwinning of fivefold twins, grain sizes also play a significant role. In Fig. 7(a), the double fivefold twins are developed inside a much larger grain during isothermal solidification of Al melt at 500 K. While tensile strain is applied in [100] direction, the grain is stretched. During the grain elongation, the GBs shrink the size of the fivefold twins. For nanocrystalline metals with average grain sizes between 10 and 100 nm, it is recognized that the competition between dislocation- and GB-mediated deformation mechanisms govern the deformation mechanism. Previous works by MD simulations suggested that GBs in nanocrystalline metals act as both source and sink for crystal defects such as dislocation, vacancy, and twins [66, 67]. The snapshots in Fig. 7 show how GBs absorb the twins as the polycrystalline Al becomes plastic (See the stress-strain plot of a typical polycrystalline sample in Fig. 6(e)).

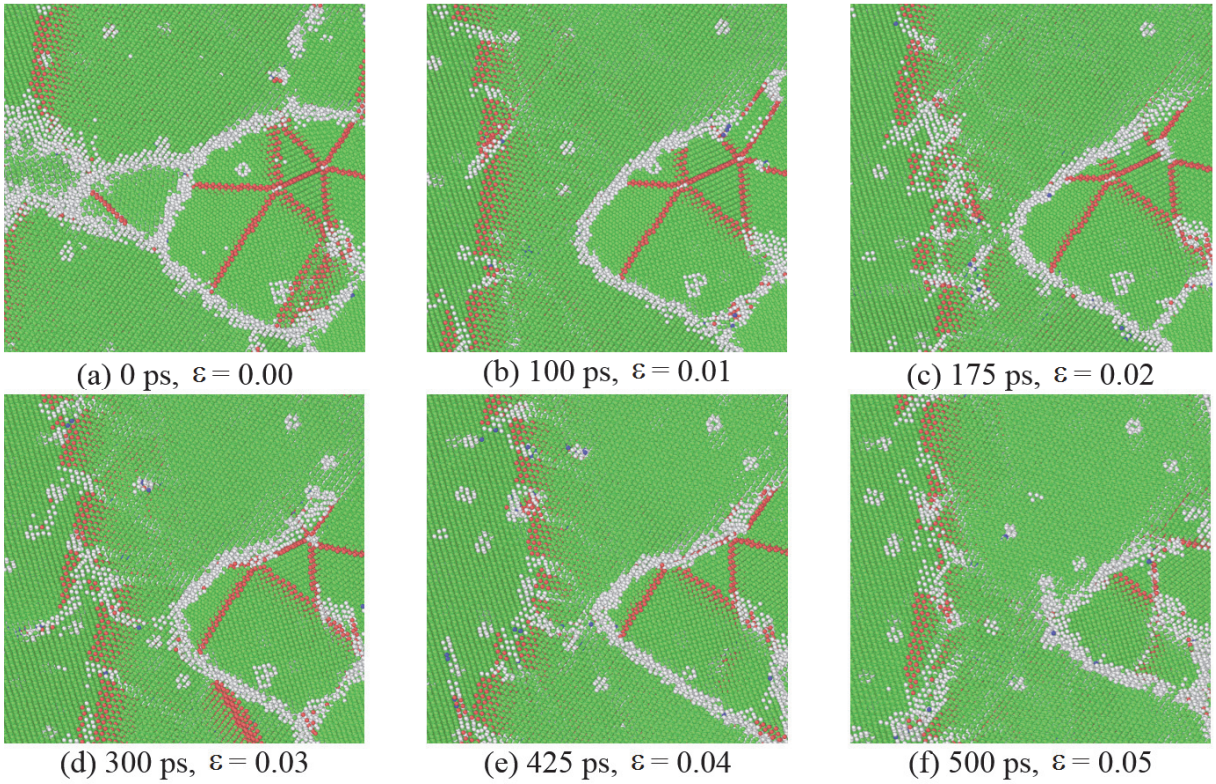


**Fig. 7.** At 500 K with a SR of $10^9$ $s^{-1}$ in the single crystal Al a twin formed and then detwinned in the direction. The sample is quenched at $10^{11}$ $Ks^{-1}$.

### 3.3 Void formation

The void formation process and the associated strain levels during the tensile deformation are shown in Fig. 8. The solid circle in Fig 8 shows the formation of a void at a GB with increasing strain. The increase of void volume in a stretched area starts during the plastic flow of polycrystalline Al. The void under tensile load generally happens due to local shear stress by the GB movement. Comparing Fig. 8(a) and (b), we see several full and partial dislocation emission at a strain of 0.16. The emission of dislocation loops from the GBs leads to void nucleation. Upon increased loading and strain, voids grow while other dislocations are consumed by increasing void and GB volumes. In general, ductile metals normally fail in monotonic loading through nucleation, growth and coalescence of voids. The evidence of ductile fracture behavior via void formation/growth at GBs has also been observed on facture surfaces by scanning electron microcopy in monocrystalline Al under uniaxial tension [68, 69].

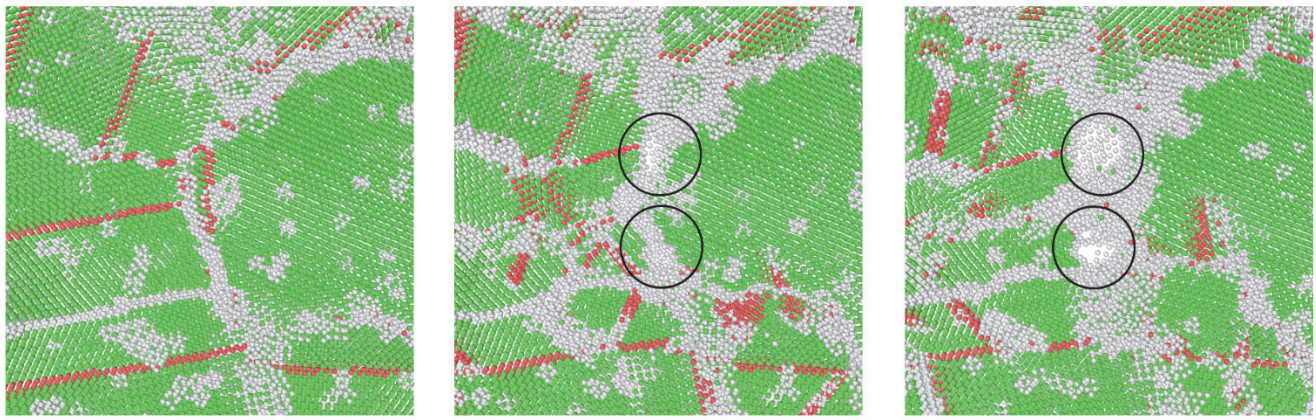


**Fig. 8.** Atomistic illustration of the onset of void under the tensile stress. The solid black circle shows formation of void at the grain boundary. The sample is solidified at 500 K, and the deformation is done at $10^9$ $s^{-1}$ at 300 K.

### 3.4 Mechanical Properties of Solidified Polycrystals

In this sub-section, we investigate the mechanical behavior of the polycrystalline Al created by solidification at different isothermal temperatures and quench rates. Utilizing uniaxial tension of polycrystalline Al samples having different solidified structures, the stress-strain plots are obtained. From these curves, the mechanical properties such as yield strength, Young's modulus, and ultimate tensile strength (UTS) are derived. The yield strength is found from the linear regression of the stress data with 0.2% offset on strain. The intersecting point of the linear fit from the regression and the actual stress-strain curve is the yield strength. No permanent deformation happens in the elastic (linear) part of the curve. The highest point in the stress-strain curve is the UTS. The inverse Hall-Petch relationship is discussed in this context of increasing yield strength with increasing grain size for solidification at higher solidification temperatures or slower quench rates (Fig. 10).

Young's modulus of the solidified polycrystalline samples is compared with that of the single crystall Al in Fig. 9(a)-(d). The expected decline of Young's modulus is observed with increasing the deformation temperature when the SR is kept constant (between $10^8$ to $10^{10}$ $s^{-1}$). A higher SR and/or a lower deformation temperature produced a stronger sample in all the cases; for example, compare cases in Fig. 9(a) with SR of $10^{10}$ $s^{-1}$ to those in Fig. 9(a) with SR of $10^8$ $s^{-1}$. In tension at 300 K and the SR of $10^{10}$ $s^{-1}$, the single crystal has a Young's modulus of ~60-65 GPa which is comparable to the previous experimental and computational results [70-72]. Under the same tensile loading conditions, the polycrystalline samples prepared by isothermal solidification at 500 K could reach a maximum Young's modulus of 58 GPa (Fig. 9 (a)). Overall the Young's modulus remains between 46-65 GPa; these values are similar to those achieved by experiments performed on nanocrystalline Al by Haque et al. [73]. Table 2 shows a comparison of the Young's modulus determined by our MDs simulations to those for single crystal and nanocrystalline experiments. The margin of error is less than 5% for Young's modulus of a single crystal Al determined by indentation test [70, 74].

Table 2. Young's modulus values at 300K for single crystal and nanocrystalline Al determined by MD calculations or experiments. The average grain size of polycrystalline cases is given in the parenthesis.

| Al Bulk | Young's Modulus (GPa) | |
|---|---|---|
| | Current MD work | Previous Results (Methods) |
| Single Crystal | 58-64 | 67.2-69.5 (Expt.) [70], 64 (MD) [72], 62.3 ± 3.1 (Expt.) [74] |
| Nanocrystalline | 40-65 (Average grain size: 5-11nm) | 67 (MD, Grain size 11.1nm) [72], 60.2 (Expt., Average grain size: 11.1nm) [73] |

The UTS for single and polycrystals are shown in Fig. 9(e) and (f). The UTS for single crystal is much higher than the polycrystalline Al. The UTS of single crystal remains between 5.5 GPa and 7.5 GPa (Fig. 9(e-f)), and when the deformation temperature increases by 200 K a decrease of strength by almost 24% is observed. However, this change in UTS in polycrystalline samples solidified isothermally or by quenching is only less than 10%; for example in Fig. 9(e) for the isothermal solidification at 500 K, the strength goes down from 3.5 GPa to 3.25 GPa from deformation temperature of 300K to 500 K. A detailed discussion of mechanical properties of nanocrystalline metals by Meyers et al. [31] shows the extremely high strength of 3.5-4 GPa for nanocrystalline Al with an average grain size between 5 nm and 10 nm. The high strength results from our MD simulations are comparable to the reported experimental data for nanocrystalline Al.

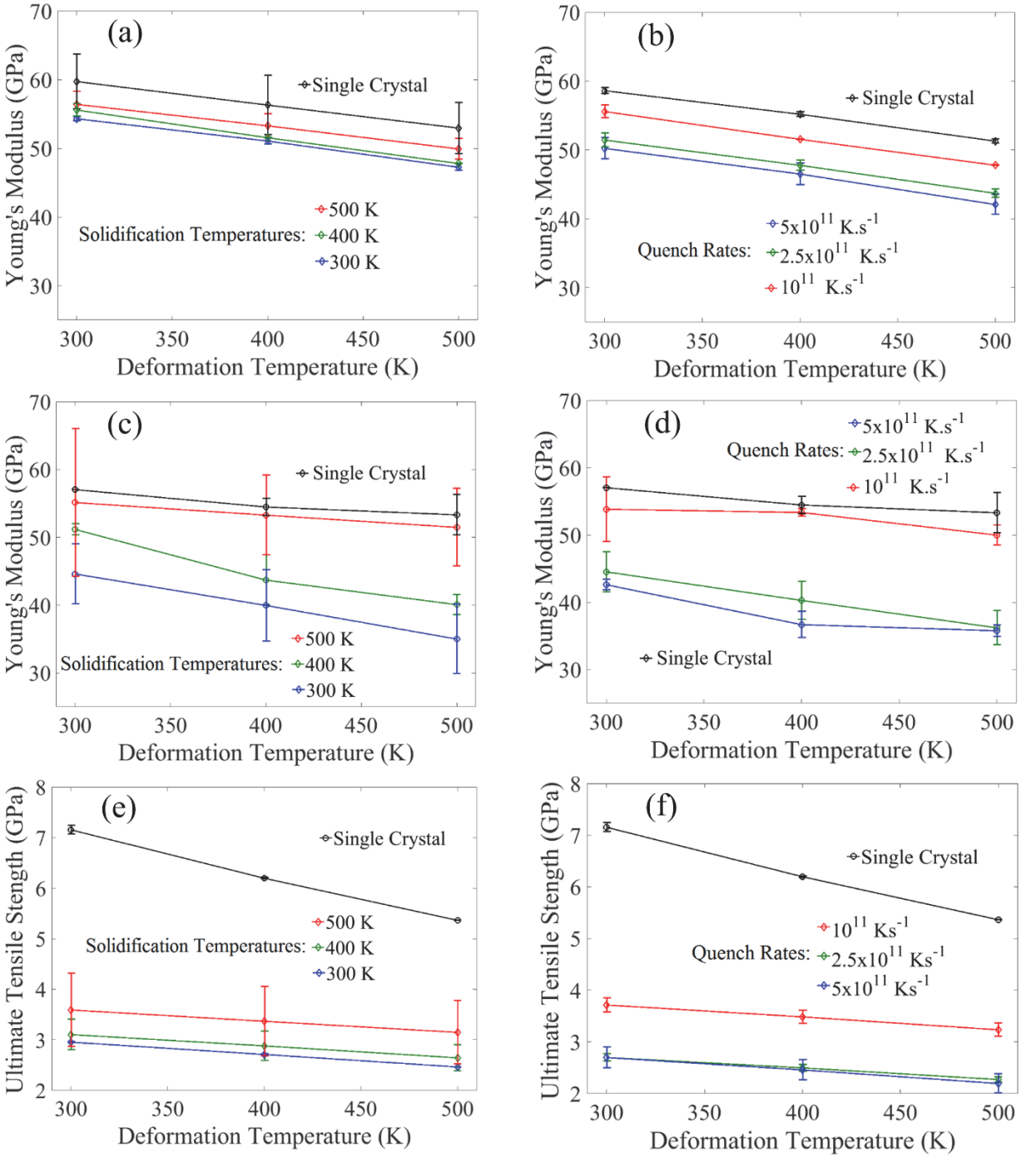


**Fig. 9.** (a) Young's modulus of isothermally solidified polycrystalline samples in tension at the SR of $10^{10}$ $s^{-1}$, (b) Young's modulus of solidified polycrystalline samples prepared by quenching in tension at the SR of $10^{10}$ $s^{-1}$. (c) Young's modulus of isothermally solidified polycrystalline samples in tension at the SR of $10^{8}$ $s^{-1}$, (d) Young's modulus of solidified polycrystalline samples prepared by quenching in tension at the SR of $10^{8}$ $s^{-1}$, (e) Ultimate tensile strength of isothermally solidified polycrystalline samples in tension at the SR of $10^{10}$ $s^{-1}$, (f) Ultimate tensile strength of solidified polycrystalline samples prepared by quenching in tension at the SR of $10^{10}$ $s^{-1}$. Single crystal results are also plotted for comparison.

The yield strength of single and polycrystals can be studied by direct relationship between the grain size of a metal and its yield strength, which is known as the Hall-Petch (HP) relation. When the grain size is above its critical value, the strength increases as the grain size decreases. At the critical grain size, the material has its maximum strength [20, 75]. Below the critical grain size, an inverse HP relationship is expected: the smaller the grain size the weaker the metal [20, 76]. This is because an alternative deformation mechanisms take over [31].

In general, the yield strength ($\sigma_y$) increases by creasing the average grain size based on the HP equation [77, 78]:

$$\sigma_y = \sigma_0 + kd^{-1/2}, \tag{1}$$

where $\sigma_0$ is a materials constant which can be calculated in the absence of GBs, $k$ is strengthening coefficient and $d$ refers to the grain size. The dislocation density becomes a more dominating factor than the total number of dislocations, so when the grain size is decreased the dislocation density increases. Due to that the dislocation pile up increases with finer grain size and the yield strength increases. However, for very small grain sizes, this mechanism will fail because grains are not able to support dislocation pile-ups. Usually for Al, this is anticipated to happen for average grain sizes below 25 nm [71]. Additionally, the shift in the HP slope usually happens for grain sizes larger than 10 nm. The inverse HP relationship is shown in Fig. 10; as the grain size increases (with increasing isothermal solidification temperature from 300K to 500K) the tensile yield strength increases for all the polycrystalline samples. The similar behavior is observed for the samples prepared by quenching; in higher quench rates resulting in smaller grain sizes, the yield strength is lower. The average grain sizes are also shown in the inset table of Fig. 10.

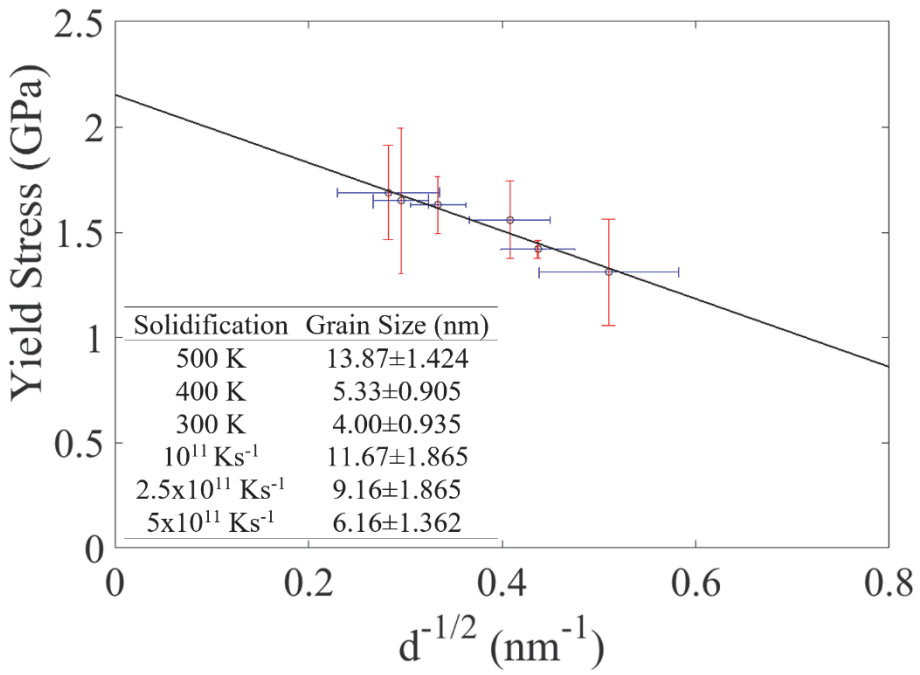


**Fig. 10.** (a) Inverse HP relationship is shown for different grain size (nm) and yield stress (GPa); data for the uniaxial tensile deformation at 300 K and the SR of $10^{10}$ $s^{-1}$ are used to plot this figure. The average grain sizes for 3 isothermal and 3 quenching solidification cases are shown in the inset table.

## 4. Conclusion

We performed MD simulations utilizing 2NN MEAM interatomic potential to study defect evolution process and deformation mechanisms of solidified polycrystalline Al under uniaxial tension. The polycrystalline Al samples were created by solidification at different quench rates and at different isothermal solidification temperatures. Several SRs and deformation temperatures were investigated. Since the GBs, vacancies, and TBs form spontaneously in arbitrary directions, the solidified polycrystalline Al was deformed in three different (100), (010) and (001) directions to account for potential statistical errors.

For all different simulations at various isothermal temperatures and cooling rates several defects such as twinning, dislocations, voids have been observed. The instability in the solidification process caused by thermal fluctuations at solid-liquid interfaces is the primary reason for twin formation. The primary Al is identified as fcc whereas the twins are hcp crystal structures. The evolution of solidification defects such as CTBs and fivefold twins were analyzed. In case of the fivefold twins, the average twin angle was ~70-73 $^{\circ}$ to form almost 360 $^{\circ}$. Ideally it should be

fully circular, but during the spontenous solidfication the nuclei are not pefectly spherical and also TBs have have a few Angstrom thickness themsleves, leaving a few degrees gap in the five-fold twins. Overall, our simulations confirm the formation of CTB and multifold twins during solidification, which is extremely difficult to observe in experiments as the entire process of layer by layer twin formation happens in the interior part of the liquid metal. During the tensile deformation, detwinning occurred for both solidification and deformation twins. The detwinning during plastic straining is more evident at higher deformation temperatures. Nucleation of voids at GBs were also observed due to the emission of dislocation loops from the GBs.

The effect of tensile testing temperature and SR was taken into account in analyzing the mechanical properties of solidified samples. The Young's modulus, yield strength, and ultimate tensile strength reduced by increasing the deformation temperature. However, the effect of SR is opposite, and the Young's modulus and ultimate tensile strength increased by increasing the SR of deformation. The uniaxial tensile strength of single crystal Al was determined to be almost twice as that of the polycrystalline Al, but single crystal Al is brittle in nature whereas the polycrystalline Al can be plastically deformed considerably. Lower quench rates and higher isothermal solidification temperatures created larger grains during solidification, and samples with larger grains showed higher yield strength and Young's modulus, and this is an indication of an Inverse Hall-Petch relationship. In the literature, there are several studies predicted the inverse Hall Petch for metals with average grain sizes less than 10 nm which is consistence with our predications.

Overall the polycrystalline model prepared by spontaneous solidification can reproduce the similar mechanical behavior of Al (i.e., dependency on temperature, SR effects, etc.) expected from experimental or other simulation studies. This also indicates that with larger computational resources the studies of polycrystalline Al and its alloys can be extended to microstructural level comparable to experimentally available data.

**Data statement**

The raw/processed data are available from the corresponding author on reasonable request.

**CRediT authorship contribution statement**

**Avik Mahata:** Writing – original draft, Methodology, Formal analysis, Visualization. **Mohsen Asle Zaeem:** Conceptualization, Methodology, Supervision, Project administration, Writing - original draft, Writing - review & editing, Funding acquisition.

**Acknowledgments**

Authors would like to acknowledge the funding support from the U.S. National Science Foundation (grant numbers: CMMI 1537170 and CMMI 1855491). Authors are grateful for the computer time allocation provided by the Extreme Science and Engineering Discovery Environment (XSEDE), award number TG-DMR140008.

## References

[1] G.E. Dieter, D.J. Bacon, Mechanical metallurgy, McGraw-Hill New York, 1986.
[2] M. Meyers, O. Vöhringer, V. Lubarda, Acta materialia, 49 (2001) 4025-4039.
[3] T. Mukhopadhyay, A. Mahata, S. Dey, S. Adhikari, Journal of Materials Science & Technology, 32 (2016) 1345-1351.
[4] M. Chen, E. Ma, K.J. Hemker, H. Sheng, Y. Wang, X. Cheng, Science, 300 (2003) 1275-1277.
[5] B. Li, B.Y. Cao, K.T. Ramesh, E. Ma, Acta Materialia, 57 (2009) 4500-4507.
[6] Y.T. Zhu, X.Z. Liao, S.G. Srinivasan, Y.H. Zhao, M.I. Baskes, F. Zhou, E.J. Lavernia, Applied Physics Letters, 85 (2004) 5049-5051.
[7] F. Zhao, L. Wang, D. Fan, B.X. Bie, X.M. Zhou, T. Suo, Y.L. Li, M.W. Chen, C.L. Liu, M.L. Qi, M.H. Zhu, S.N. Luo, Physical Review Letters, 116 (2016) 075501.
[8] M. Avik, M. Tanmoy, A. Sondipon, Materials Research Express, 3 (2016) 036501.
[9] K. Dragnevski, R. Cochrane, A. Mullis, Metallurgical and Materials Transactions A, 35 (2004) 3211-3220.
[10] M.A. Salgado-Ordorica, M. Rappaz, Acta Materialia, 56 (2008) 5708-5718.
[11] S. Henry, M. Rappaz, P. Jarry, Metallurgical and Materials Transactions A, 29 (1998) 2807-2817.
[12] J. Li, F. Seki, S. Saimoto, K. Itoh, T. Kamijo, Scripta Materialia, 36 (1997) 1261-1266.
[13] D. Field, L. Bradford, M. Nowell, T. Lillo, Acta materialia, 55 (2007) 4233-4241.
[14] Q. Li, J. Cahoon, N. Richards, Scripta materialia, 55 (2006) 1155-1158.
[15] T. Duffar, 5 (2010) 61-113.
[16] N. Iqbal, N.H. van Dijk, S.E. Offerman, M.P. Moret, L. Katgerman, G.J. Kearley, Acta Materialia, 53 (2005) 2875-2880.
[17] B. Li, H.D. Brody, D.R. Black, H.E. Burdette, C. Rau, Journal of Physics D: Applied Physics, 39 (2006) 4450.
[18] G. Zeng, K. Nogita, S. Belyakov, J. Xian, S. McDonald, K. Yang, H. Yasuda, C. Gourlay, Real-Time Observation of AZ91 Solidification by Synchrotron Radiography, in: Magnesium Technology 2017, Springer, 2017, pp. 597-603.
[19] A. Tandjaoui, N. Mangelinck-Noel, G. Reinhart, B. Billia, X. Guichard, Comptes Rendus Physique, 14 (2013) 141-148.
[20] D. Wolf, V. Yamakov, S. Phillpot, A. Mukherjee, H. Gleiter, Acta Materialia, 53 (2005) 1-40.
[21] Y. Xu, B. Yan, H.-J. Zhang, J. Wang, G. Xu, P. Tang, W. Duan, S.-C. Zhang, Physical review letters, 111 (2013) 136804.

[22] D. Gianola, S. Van Petegem, M. Legros, S. Brandstetter, H. Van Swygenhoven, K. Hemker, Acta Materialia, 54 (2006) 2253-2263.
[23] D.E. Spearot, K.I. Jacob, D.L. McDowell, Acta Materialia, 53 (2005) 3579-3589.
[24] K. Aust, F. Krill, F.R. Morral, Journal of Metals, 4 (1952) 865-866.
[25] H. Fredriksson, M. Hillert, Journal of Materials Science, 6 (1971) 1350-1354.
[26] W. Han, G. Cheng, S. Li, S. Wu, Z. Zhang, Physical review letters, 101 (2008) 115505.
[27] Y.F. Shao, S.Q. Wang, Scripta Materialia, 62 (2010) 419-422.
[28] E. Bringa, D. Farkas, A. Caro, Y. Wang, J. McNaney, R. Smith, Scripta Materialia, 59 (2008) 1267-1270.
[29] P. Huang, G. Dai, F. Wang, K. Xu, Y. Li, Applied Physics Letters, 95 (2009) 203101.
[30] T. Shen, Y. Wu, X. Lu, Journal of molecular modeling, 19 (2013) 751-755.
[31] M.A. Meyers, A. Mishra, D.J. Benson, Progress in materials science, 51 (2006) 427-556.
[32] F. Zhao, L. Wang, D. Fan, B. Bie, X. Zhou, T. Suo, Y. Li, M. Chen, C. Liu, M. Qi, Physical review letters, 116 (2016) 075501.
[33] F.-f. Zhu, W.-j. Chen, Y. Xu, C.-l. Gao, D.-d. Guan, C.-h. Liu, D. Qian, S.-C. Zhang, J.-f. Jia, Nature materials, 14 (2015) 1020-1025.
[34] E. Asadi, M. Asle Zaeem, S. Nouranian, M.I. Baskes, Acta Materialia, 86 (2015) 169-181.
[35] V. Yamakov, D. Wolf, S. Phillpot, H. Gleiter, Acta Materialia, 50 (2002) 5005-5020.
[36] J. Schiotz, F.D. Di Tolla, K.W. Jacobsen, Nature, 391 (1998) 561.
[37] S. Kibey, J. Liu, D. Johnson, H. Sehitoglu, Acta materialia, 55 (2007) 6843-6851.
[38] B. Li, M. Sui, B. Li, E. Ma, S. Mao, Physical review letters, 102 (2009) 205504.
[39] R.-Z. Qiu, C.-C. Li, T.-H. Fang, Physica Scripta, 92 (2017) 085702.
[40] F. Zhang, Z. Liu, J. Zhou, Materials Letters, 183 (2016) 261-264.
[41] A. AlMotasem, J. Bergström, A. Gåård, P. Krakhmalev, L. Holleboom, Tribology letters, 65 (2017) 101.
[42] H. Van Swygenhoven, A. Caro, D. Farkas, Materials Science and Engineering: A, 309-310 (2001) 440-444.
[43] B.-J. Lee, M. Baskes, Physical Review B, 62 (2000) 8564.
[44] E. Asadi, M. Asle Zaeem, S. Nouranian, M.I. Baskes, Physical Review B, 91 (2015) 024105.
[45] E. Asadi, M. Asle Zaeem, Acta Materialia, 107 (2016) 337-344.
[46] A. Mahata, M. Asle Zaeem, M.I. Baskes, Modelling and Simulation in Materials Science and Engineering, 26 (2018) 025007.
[47] A. Stukowski, Modelling and Simulation in Materials Science and Engineering, 18 (2009) 015012.
[48] H. Tsuzuki, P.S. Branicio, J.P. Rino, Computer physics communications, 177 (2007) 518-523.
[49] M. Parrinello, A. Rahman, Journal of Applied physics, 52 (1981) 7182-7190.
[50] S. Plimpton, Journal of Computational Physics, 117 (1995) 1-19.
[51] M. Ball, D. Lloyd, Scripta metallurgica, 19 (1985) 1065-1068.
[52] J. Narayan, Journal of Materials Research, 5 (1990) 2414-2423.
[53] M. Bhogra, U. Ramamurty, U.V. Waghmare, Journal of Physics: Condensed Matter, 26 (2014) 385402.
[54] L. Liu, R. Wang, X. Wu, L. Gan, Q. Wei, Computational Materials Science, 88 (2014) 124-130.
[55] H. Hofmeister, Crystal Research and Technology, 33 (1998) 3-25.
[56] A.J. Cao, Y.G. Wei, Applied Physics Letters, 89 (2006) 041919.
[57] Y.T. Zhu, X.Z. Liao, R.Z. Valiev, Applied Physics Letters, 86 (2005) 103112.
[58] Q. Qin, S. Yin, G. Cheng, X. Li, T.-H. Chang, G. Richter, Y. Zhu, H. Gao, Nature communications, 6 (2015) 5983.
[59] Z.L. Wang, Particle & Particle Systems Characterization: Measurement and Description of Particle Properties and Behavior in Powders and Other Disperse Systems, 18 (2001) 142-165.
[60] X. An, Q. Lin, S. Wu, Z. Zhang, R. Figueiredo, N. Gao, T. Langdon, Scripta Materialia, 64 (2011) 249-252.
[61] A. Cao, Y. Wei, Applied physics letters, 89 (2006) 041919.

[62] S. Lee, J. Im, Y. Yoo, E. Bitzek, D. Kiener, G. Richter, B. Kim, S.H. Oh, Nature Communications, 5 (2014) 3033.
[63] J. Wang, N. Li, O. Anderoglu, X. Zhang, A. Misra, J.Y. Huang, J.P. Hirth, Acta Materialia, 58 (2010) 2262-2270.
[64] J. Li, J. Zhang, L. Jiang, P. Zhang, K. Wu, G. Liu, J. Sun, Materials Science and Engineering: A, 628 (2015) 62-74.
[65] S. Ogata, J. Li, S. Yip, Physical Review B, 71 (2005) 224102.
[66] J. Schiøtz, K.W. Jacobsen, Science, 301 (2003) 1357-1359.
[67] V. Yamakov, D. Wolf, S. Phillpot, A. Mukherjee, H. Gleiter, Nature materials, 3 (2003) nmat1035.
[68] H.J. Choi, S.W. Lee, J.S. Park, D.H. Bae, Scripta Materialia, 59 (2008) 1123-1126.
[69] A.A. Benzerga, J.-B. Leblond, Ductile fracture by void growth to coalescence, in: Advances in applied mechanics, Elsevier, 2010, pp. 169-305.
[70] J.-C. Kuo, I.-H. Huang, Materials transactions, 51 (2010) 2104-2108.
[71] W. Xu, L.P. Dávila, Materials Science and Engineering: A, 710 (2018) 413-418.
[72] W. Xu, L.P. Dávila, Materials Science and Engineering: A, 692 (2017) 90-94.
[73] M. Haque, M.A. Saif, Scripta Materialia, 47 (2002) 863-867.
[74] S.-H. Kim, H.-K. Kim, J.-H. Seo, D.-M. Whang, J.-P. Ahn, J.-C. Lee, Acta Materialia, 160 (2018) 14-21.
[75] T. Nieh, J. Wadsworth, Scripta Metallurgica et Materialia, 25 (1991) 955-958.
[76] C. Carlton, P. Ferreira, in: Acta Materialia, 2007, pp. 3749-3756.
[77] J. Schiøtz, F.D. Di Tolla, K.W. Jacobsen, Nature, 391 (1998) 561.
[78] S. Yip, Nature, 391 (1998) 532.